SI APPENDIX

Aljoscha Nern, Barret D. Pfeiffer and Gerald M. Rubin

"Optimized tools for multicolor stochastic labeling reveal diverse stereotyped cell arrangements in the fly visual system"

SI Methods

Construction of pJFRC smGFP reporter vectors: Gene sequences were codon optimized for Drosophila using Gene Designer ((1); software available from DNA2.0, Inc., Menlo Park, CA). The smGFP-HA, -cMyc, -V5, -FLAG, -OLLAS, -StrepTag2 genes were synthesized by DNA2.0 and cloned 5′-*Bam*HI to 3′-*Xba*I into pJFRC12-10XUAS-IVS-myr::GFP (2), replacing the GFP reporter, to generate 10XUAS constructs (pJFRC200, pJFRC202, pJFRC205, pJFRC207, pJFRC209 and pJFRC211). Next, myr::smGFP transgene fusions were liberated as *Xho*I to *Xba*I fragments and cloned into pJFRC5-5XUAS-IVS-mCD8::GFP (2) after removal of mCD8::GFP resulting in 5XUAS variants (pJFRC199, pJFRC204 and pJFRC225). A FRT-flanked "stop cassette" consisting of an early SV40 transcriptional terminator (>STOP>) was cloned 5′-*Bgl*II to 3′-*Xho*I into the 10XUAS-IVS-myr::smGFP reporters after removal of the IVS (pJFRC201, pJFRC203, pJFRC206, pJFRC208, pJFRC210 and pJFRC212). Alternative "stop cassettes" flanked with recognition target sites for KD and B3 recombinases (3) were cloned in a similar manner (pJFRC226-pJFRC232). Constructs in 13XLexAop2 vectors (2), (pJFRC213 - pJFRC224) were generated essentially as described above for UAS constructs. Transgenic fly lines were generated by Genetic Services, Inc.

Construction of pJFRC239-242 tandem vectors: Methods used were identical to those described previously (2) in a multi-step process. First, 10XUAS-IVS-myr::sfGFP (superfolderGFP; (4)), pJFRC206, and pJFRC208 (see Table S1) were cut with *Fse*I, followed by ligation with a 2.8kb gypsy-insulated spacer (2), and PCR screened for orientation. Next, the vectors were cut with *Pme*I and ligated with a *Hind*III (blunt) to *Pme*I-cut and gel extracted 10XUAS-FRT>STOP>FRT-myr::smGFP-HA, -cMyc, or –FLAG (pJFRC201, pJFRC203, and pJFRC208, respectively) fragment. More than 96 bacterial colonies were PCR screened for stability and orientation; PCR-positive clones were confirmed by examination of *Xba*I digests.

Construction of smGFP-V5, -HA, and -OLLAS polarity reporters: C-terminal fusions of smGFPs with Drosophila synaptotagmin (Syt1) followed the general strategy of (5) as follows: First, the coding sequence for synaptotagmin, based on cDNA clone GH14933 (Genbank Accession #BT004498; (6)) was altered to remove internal *Kpn*I and *Bam*HI restriction sites, synthesized to include a 7-bp translation-initiation sequence (2, 3) and flanked by 5′-*Xho*I to 3′-*Bam*HI sites. Next, the synthesized synaptotagmin gene was cut 5′-*Xho*I to 3′-*Bam*HI and cloned as a triple ligation with 5′-*Bam*HI to 3′-*Xba*I smGFP-HA or smGFP-V5 into 5′-*Xho*I to 3′-*Xba*I cut pJFRC4-3XUAS-IVS vector (2) resulting in pJFRC51 and pJFRC123. A Syt::smGFP-HA transgene fusion was liberated from pJFRC51-3XUAS-IVS-Syt::smGFP-HA by digesting with 5′-*Xho*I to 3′-*Xba*I and ligating into similarly cut pJFRC5-5XUAS-IVS and pJFRC18-8XLexAop2 (2) vectors to produce pJFRC122-5XUAS-IVS-Syt::smGFP-HA and pJFRC47-8XLexAop2-Syt::smGFP-HA, respectively. Repeating the general design from above, a triple ligation of a synthesized synaptotagmin gene cut 5′-*Xho*I to 3′-*Bam*HI with 5′-*Bam*HI to 3′-*Xba*I smGFP-OLLAS into 5′-*Xho*I to 3′-*Xba*I cut pJFRC18-8XLexAop2 vector resulted in pJFRC46-8XLexAop2-Syt::smGFP-OLLAS. A 5XUAS-DenMark-mCherry construct was generated in a multistep fashion from PCR using UAST-DenMark (gift of Bassem Hassan; (7)) as template. First, a triple ligation consisting of a 5′-*Not*I to 3′-*Kpn*I PCR fragment spanning the first 2515bps of DenMark with a 286bp 5′-*KpnI* to 3′-*Xba*I PCR fragment of the 3′ end of Denmark was cloned into a 5XUAS vector as 5′-*Not*I to 3′-*Xba*I. Next mCherry was PCR amplified from UAS-DenMark with flanking 5′ and 3′ *Kpn*I restriction sites and cloned into 5XUAS-DenMark vector allowing for modularity in choice of fluorescent protein. pJFRC120-5XUAS-DenMark-smGFP-V5 was made by removal of mCherry from 5XUAS-DenMark and replacement with a *Kpn*I digested PCR product of smGFP-V5 screened for orientation and sequence verified. DenMark-smGFP-V5 was then liberated from pJFRC120 as a 5′-*Not*I to 3′-*Xba*I fragment and cloned into a 3XUAS vector to make pJFRC121.

Construction of Flp drivers: R57C10-Flp2::PEST was constructed by first digesting R57C10-GAL4 DNA (8) 5′-*Kpn*I to 3′-*Spe*I removing the yeast GAL4 CDS and *hsp70* terminator. Next, a 5′-*Kpn*I to 3′-*Spe*I digest of pBPFlp2::PESTw destination vector was performed to extract a fusion of Drosophila codon-optimized Flippase2 with the mODC PEST sequence (3) and *hsp70* transcriptional terminator (2). Ligation of Flp2::PEST as a 5′-*Kpn*I to 3′-*Spe*I into the parent R57C10 digested DNA resulted in R57C10-Flp2::PEST which included an unique restriction site, *Avr*II, 5′ to the *Hind*III and *hsp70* terminator (See (9)). PCR amplicons of yeast Flp2 and FlpL (10) were amplified from pUAS-Flp (3) and pJFRC79-8XLexAop2-FlpL (11) templates, respectively, digested as 5′-*Kpn*I to 3′-*Avr*II fragments, and ligated into a similarly digested R57C10 vector after removal of Flp2::PEST to produce R57C10-Flp2 and R57C10-FlpL. PCR amplification of FlpL was repeated, but with a 5′ primer that mutated the 5th amino acid from Aspartic Acid to Glycine, and cloned as a 5′-*Kpn*I to 3′-*Avr*II fragment into the parent R57C10 vector to yield R57C10-FlpL2, a weaker Flp driver version of R57C10-FlpL.

Construction of pBPhsFlp2::PEST was performed in a manner similar to that previously described (3). Coding sequence for Flp2::PEST was PCR amplified as a 5′-*Kpn*I to 3′-*Avr*II fragment from R57C10-Flp2::PEST, to include a 7-bp translation-initiation sequence, and cloned into pBPhsFlp2 replacing the Flp2 transgene.

Construction of pJFRC Flp responders: To create pJFRC134 - pJFRC141 and pJFRC144 - pJFRC149, all flippase variants—Flp2, FlpL,

FlpL2, Flp2-Rs (*Rhodobacter sphaeroides* codon usage), and Flp2-At (*Arabidopsis thaliana* codon usage)—were PCR cloned as 5′-*Xho*I to 3′-*Xba*I fragments into vectors containing 1-5XUAS sites and either a *hsp70* or DSCP promoter as previously described (2).

Construction of R29C07-KD::Geneswitch driver: In order to make R29C07 KD::Geneswitch-4, we initially built a gateway compatible destination vector. First, a triple ligation was performed with 5′-*Nhe*I to 3′-*Bam*HI PCR amplified KD recombinase (3), a 5′- *Bam*HI to 3′-*Hind*III PCR amplified codon-optimized GeneSwitch (12-14), into a 5′-*Nhe*I to 3′- *Hind*III cut pBPivsFlp1Uw destination vector after removal of the Flp1 transgene. Next, pJFRC14 (2) was digested with *Hind*III to extract the WPRE element, subsequently cloned into *Hind*III-digested pBPivsKD::GeneswitchUw, and PCR screened for direction yielding pBPKD::GeneSwitchUw-4 (pBPivsKD::GeneSwitchWPREUw; for nomenclature see (2). Lastly, CRM R29C07 which had previously been PCR cloned in pENTR/D-TOPO was transferred, using gateway LR recombinase, into pBPKD::GeneSwitchUw-4 (9) to produce R29C07-KD::GeneSwitch-4.

Construction of Tubulin "Flp-Off," "Blown-Off," and "Kicked-Off" GAL80 drivers: First, Flpd-OUT, Blown-OUT, and Kickd-OUT Stop cassettes (3) were PCR amplified as 5′-*Kpn*I to 3′-*Hind*III fragments and cloned into a modified pBDPGAL4U vector (9). Second, pBPGAL80Uw-6 (2) was used as template to amplify the IVS, Drosophila codon-optimized GAL80, and WPRE as 5′-*Age*I to 3′-*Mlu*I fragments which were digested and ligated into the similarly digested pBDP-Flpd-OUT, Blown-OUT, and Kickd-OUT vectors after removal of their internal *hsp70* transcriptional terminator. Finally, the 2,613bp tubulin promoter (gift of Tzumin Lee; (15)) was PCR amplified with flanking *Eco*RI restriction sites, digested, cloned into the modified vectors above, and PCR screened for correct orientation resulting in tubP-FRT>GAL80-6-FRT>, tubP-B3RT>GAL80-6-B3RT>, and tubP-KDRT>GAL80-6-KDRT>.

Drosophila Genetics: Standard techniques were used for fly stock maintenance and construction. Individual transgenic fly lines (except GAL4 and LexA drivers) are listed in Table S1, stocks with combinations of multiple transgenes in Table S2, and GAL4 (16, 17), split-GAL4 and LexA driver lines in Table S3. LexA transgenes were constructed as described (2). The tables also provide details on which fly lines were used for specific experiments (Tables S2 and S3) and the relevant expression patterns of the GAL4 and LexA lines (Table S3). All listed GAL4 and LexA lines are also expressed in several other cell populations but are sufficiently specific to unambiguously identify the indicated Dm and Pm neuron types. New cell types were named by extending the naming scheme of Fischbach and Dittrich (18). References to described Dm cell types are included in Table S4. Pm4 appears to be identical to "Pm_{910}" (19) and "Mi_{new1}"(20). All experiments in this study were done with female flies.

Preparation of flies for MCFO labeling: Stocks with combinations of MCFO cassettes and Flp-recombinase drivers (Table S2) were crossed to the appropriate GAL4 driver lines (Table S3) and the progeny raised at 25°C. For temperature-induced expression of Flp, larval or adult flies were placed in vials with culture medium and incubated in a 37°C water bath for 12 min to 1 hr. With pBPhsFlp2::PEST in attP3 as the Flp source, 12-15 min and 30-40 heat-shocks are suitable starting points for sparse or dense labeling of neurons with many GAL4 driver lines. With the exception of the experiments shown in Fig. 2D,E, in which Flp was induced at the first instar larval stage, all heat-shock treatments were of adult flies. Flies were dissected two or more days after Flp-induction. R57C10 driven Flp drivers do not require a temperature-shift for Flp-induction. With these drivers, dissection of flies at different ages permits some adjustment of labeling frequencies (older flies have more stop-cassette excision events). For sparse labeling of neurons from the R57C10 pattern, pJFRC137-1XUAS-IVS-FlpL2 in attP40/+; R57C10-GAL4/HA_V5_FLAG (used for Fig 3E) adult flies were dissected without heat-shock and pBPhsFlp2::PEST in attP3/+; OL-KD (29C07-KDGeneswitch-4) in attP40/+; R57C10-GAL4 in attP2 tubP-KDRT>GAL80-6-KDRT> in VK00027/ HA_V5_FLAG (used for Figs. 3G,G′;4A″,B″,C″;5A [all except Dm14,Dm17,Dm19,Dm20];S2;S3) (also see Table S2) flies were heat-shocked for 60 min at the adult stage.

Immunohistochemistry: Fly brains were dissected in cold S2 cell culture medium (Schneider's Insect Medium, Sigma Aldrich, #S0146) and fixed with 2% (w/v) paraformaldehyde (PFA) (prepared from a 20% stock solution, Electron Microscopy Sciences, #15713) in S2 medium for 55 min at room temperature (RT). Fixed brains were washed 4 x 10 min with PBT [PBS with 0.5% (v/v) Triton X-100 (Sigma Aldrich, # X100)] then blocked with PBT-NGS (5% Goat Serum [Life Technologies, #16210-064] in PBT) for 1.5 hr at RT. Dissection and fixation in cell culture medium improves the preservation of fine neuronal processes. Shorter PBT-NGS blocking times (~ 30 min) were used in some experiments.

For rapid, same day assessment of stochastic labeling densities in MCFO experiments, brains were incubated with DyLight549-conjugated anti-V5 (V5-TAG SV5-Pk1 mouse MAb, DyLight 549 conjugate, AbD Serotec MCA1360D549; 1:300 dilution) for 1 hr followed by 3-4 PBT washes.

For labeling of three MCFO markers (HA, V5, FLAG) plus a reference pattern (anti-Bruchpilot (brp), (21)), brains were incubated with anti-Brp (nc82 mouse mAb, Developmental Studies Hybridoma Bank [DSHB]; supernatant at 1:30 dilution), anti-HA (C29F4 rabbit mAb, Cell Signaling Technologies #3724S, Inc.; 1:300) and anti-FLAG (DYKDDDDK Epitope Tag Antibody [L5] rat mAb, Novus Biologicals #NBP1-06712; 1:200) in PBT-NGS for 4 hr at RT followed by 4°C overnight. Samples were washed 3x 30 min with PBT, incubated with secondary antibodies (Alexa Fluor 594 Donkey anti-rabbit, Jackson Immuno Research #711-585-152 at 1:500; Alexa Fluor 647 Donkey anti-rat, #712-605-153 at 1:150; Alexa Fluor 488 Donkey anti-mouse, #715-545-151at 1:400; all diluted in PBT-NGS) for 4 hr at RT followed by 1-2 overnights at 4°C and washed with PBT as above. After an additional blocking step with PBT-NMS [5% Normal Mouse Serum (NMS) (Jackson ImmunoResearch Laboratories, Inc. #015-000-120) in PBT] for 1.5 hr at RT, brains were incubated at 4°C overnight with DyLight 549-conjugated anti-V5 (1:500) and again washed with PBT. For visualization of three MCFO markers without a reference pattern, anti-Brp was omitted and Alexa Fluor 594 Donkey anti-rabbit replaced with Alexa Fluor 488 Donkey anti-rabbit (Jackson ImmunoResearch Laboratories, Inc. # 711-545-152; 1:500).

For visualization of four MCFO labels (HA,V5,FLAG,OLLAS), three color MCFO labeling without anti-Brp was carried out as described above. Fly brains were then incubated with 0.05% (w/v) Streptavidin (Thermo Fisher Scientific Inc., #21125) in PBT-NRS (PBT with 5% (v/v) Normal Rat Serum [Jackson Immuno Research Laboratories, Inc., #012-000-120]) for 30 min to block endogenous biotin, washed 4x 15 min in PBT, incubated with 0.005% (w/v) biotin (Thermo Fisher Scientific Inc., #29129) in PBT for 15 min to block unoccupied biotin binding sites on streptavidin and washed again 4x with PBT. After overnight incubation at 4°C with biotin-anti-OLLAS (OLLAS Epitope Tag Antibody (L2) [Biotin], Novus Biologicals NBP1-06713B; 1:30 dilution) in PBT-NRS and 4x 15 min washes with PBT, samples were incubated with DyLight 594-labeled Streptavidin (DyLight 594-conjugated Streptavidin, Jackson Immuno Research Laboratories #016-580-084, Inc.; 1:100 dilution) overnight at 4°C and washed with PBT.

Visualization of GAL4 expression patterns used anti-HA (to detect pJFRC200-10XUAS-IVS-myr::smGFP-HA) with anti-Brp or anti-Chaoptin (22)(24B10 mouse mAb, DSHB, 1:20) as a reference marker. For additional LexA-labeling (with pJFRC216-13XLexAop2-IVS-myr::smGFP-V5 as reporter), brains were further blocked with PBT-NMS and incubated with DyLight 549-conjugated anti-V5 as described above.

Most immunostainings in this study were carried out in Protein LoBind Tubes (Eppendorf, #022431102) with ~10 brains in a volume of ~200 µl for antibody incubations and 1-2 ml for washing steps. For small numbers of brains with sparse labeling much smaller volumes (e.g. 10 µl) can be sufficient. With the above antibody dilutions, some samples with dense labeling of many neurons and strong marker expression showed non-uniform labeling, perhaps due to antibody depletion. In those cases, increasing primary and secondary antibody concentrations or incubation volumes produced more complete labeling. In this study, this was only done for the samples in Figs. 1G,G' and 2A-D (dilutions of all primary and secondary antibodies for MCFO markers were reduced to 1:100 in these experiments).

In some experiments, other secondary antibodies with dyes similar to those mentioned above (e.g. with DyLight 594 instead of Alexa Fluor 594) were used. DyLight 549-conjugated anti-V5 is currently no longer commercially available but may be replaced with the similar DyLight 550 conjugate (AbD Serotec MCA1360D550GA).

Mounting of labeled brains for imaging: Brains were either mounted in SlowFadeGold (Life Technologies S36937) (Figs. 1;3A-C; 4A-C;6A'-I'; 8D,H; S4A-P; S5; S8A'-D'; S9 (all except F',G',H'),S10A-D) or DPX (Sigma Aldrich #06522) (all other Figs.). SlowFade permits remounting of specimens in different orientations and provides a faster procedure if full tissue transparency is not required. DPX mounting results in highly transparent specimens and superior image quality, particularly in deeper optical sections. In addition, DPX-embedded specimens can be stored at room temperature in the dark for several months. The dehydration required for DPX mounting results in some tissue shrinkage relative to SlowFade mounted samples. In some Figures with images of both DPX and Slowfade-mounted specimens, the two groups are shown at slightly different scale in order to show similar fields of view. Scale bars were not corrected for tissue shrinkage and therefore reflect the actual dimensions of each specimen.

DPX mounting procedure: Following completion of immunostaining, brains were further fixed with 4% PFA in PBS for 4 hr at RT followed by 4 x 15 min washes with PBT. The purpose of this post-fixation step is to increase tissue stability during subsequent dehydration and clearing. The posterior surface of post-fixed brains was attached to Poly-L-lysine (PLL)-coated number 1 coverslips (see below) while the brains were submerged in PBS. Brains were dehydrated in an ethanol series (30%, 50%, 70% , 95%, 100%, 100%, 100%; all (v/v); 10 min per step), cleared in xylene (100%,100%,100%, 5 min per step). Brains were then embedded in DPX, as follows: ~7 drops of DPX were applied to the PLL-coverslip to cover the attached brains and the coverslip inverted and gently placed on a slide with two number 2 coverslips as spacers. The DPX medium was allowed to cure at RT for at least 24 hr and any DPX on the outer surface of the coverslip was removed prior to imaging. Some specimens were processed with an earlier version of this protocol in which brains were partly dehydrated (to 95% ethanol) prior to being attached to PLL slides while in 95% ethanol.

For PLL-coating, coverslips were briefly immersed in a solution of 0.08% (w/v) Poly-L-lysine (Poly-L-lysine hydrobromide, Sigma Aldrich, #P1524) and 0.2% (v/v) Kodak Photo-Flo 200 (Electron Microscopy Sciences #74257) in water and air-dried. This process can be repeated to increase adhesiveness, if required.

Microscopy and Image processing and analysis: Images were acquired on a Zeiss LSM 710 confocal microscope with 488 nm, 561 nm, 594 nm and 633 nm laser lines. Objectives used were Plan Apochromat 63x DIC NA 1.4 (most images) and Neofluor 40x DIC NA 1.3 (Figs. 1E,F,G; 2A,B,C). Samples used for generating reoriented image views (see below) were acquired as stacks with 0.38 µm z-spacing. With the exception of the anti-Brp reference channel, detector gain and laser power were kept constant for all sections of a confocal stack.

Some four channel images were acquired as two separate confocal stacks; each with the Alexa Fluor 488-labeled reference pattern plus either the Alexa Fluor 594 or the DyLight 549 and Alexa Fluor 647 channels. This protocol is faster because it reduces the need for mechanical switches between filter sets. Stacks imaged this way were combined ("blended") in a custom image processing pipeline within the Janelia Workstation set of image analyses tools (23). This pipeline also includes routines for automatic segmentation of neurons and image alignment based on the anti-Brp reference pattern (24, 25). Segmented neurons are shown in Figs. 4A",B",C", 5A and S7. Since automatic segmentation can result in fused or fragmented neurons in addition to complete cells, correct segmentation of all neurons shown was confirmed by visual inspection of the unsegmented images. Different views of segmented

neurons or complete labeling patterns from three-dimensional images were generated in the NeuronAnnotator mode of Vaa3D (26). Reoriented substack projection images for Figures were exported from NeuronAnnotator as TIFF format screen shots. In a few cases, segmentations were manually edited using Adobe Photoshop. Other image processing included adjustments of brightness and contrast of individual channels (performed in NeuronAnnotator or Fiji (http://fiji.sc/)). To show images in consistent orientation, some images were rotated or flipped horizontally to match views of left and right optic lobes. Images from the Janelia FlyLight collection (generated as described in (16)) were used to examine cell body distributions and to determine approximate cell counts (done manually on stacks viewed in Fiji). Figures were assembled using Adobe CS5 software (Indesign, Illustrator and Photoshop).

SI References

1. Villalobos A, Ness JE, Gustafsson C, Minshull J, & Govindarajan S (2006) Gene Designer: a synthetic biology tool for constructing artificial DNA segments. *BMC bioinformatics* 7:285.
2. Pfeiffer BD, *et al.* (2010) Refinement of tools for targeted gene expression in Drosophila. *Genetics* 186(2):735-755.
3. Nern A, Pfeiffer BD, Svoboda K, & Rubin GM (2011) Multiple new site-specific recombinases for use in manipulating animal genomes. *Proceedings of the National Academy of Sciences of the United States of America* 108(34):14198-14203.
4. Pedelacq JD, Cabantous S, Tran T, Terwilliger TC, & Waldo GS (2006) Engineering and characterization of a superfolder green fluorescent protein. *Nat Biotechnol* 24(1):79-88.
5. Zhang YQ, Rodesch CK, & Broadie K (2002) Living synaptic vesicle marker: synaptotagmin-GFP. *Genesis* 34(1-2):142-145.
6. Stapleton M, *et al.* (2002) The Drosophila gene collection: identification of putative full-length cDNAs for 70% of D. melanogaster genes. *Genome research* 12(8):1294-1300.
7. Nicolai LJ, *et al.* (2010) Genetically encoded dendritic marker sheds light on neuronal connectivity in Drosophila. *Proceedings of the National Academy of Sciences of the United States of America* 107(47):20553-20558.
8. Pfeiffer BD, Truman JW, & Rubin GM (2012) Using translational enhancers to increase transgene expression in Drosophila. *Proceedings of the National Academy of Sciences of the United States of America* 109(17):6626-6631.
9. Pfeiffer BD, *et al.* (2008) Tools for neuroanatomy and neurogenetics in Drosophila. *Proceedings of the National Academy of Sciences of the United States of America* 105(28):9715-9720.
10. Buchholz F, Ringrose L, Angrand PO, Rossi F, & Stewart AF (1996) Different thermostabilities of FLP and Cre recombinases: implications for applied site-specific recombination. *Nucleic Acids Res* 24(21):4256-4262.
11. Pan Y, Meissner GW, & Baker BS (2012) Joint control of Drosophila male courtship behavior by motion cues and activation of male-specific P1 neurons. *Proceedings of the National Academy of Sciences of the United States of America* 109(25):10065-10070.
12. Wang Y, O'Malley BW, Jr., Tsai SY, & O'Malley BW (1994) A regulatory system for use in gene transfer. *Proceedings of the National Academy of Sciences of the United States of America* 91(17):8180-8184.
13. Osterwalder T, Yoon KS, White BH, & Keshishian H (2001) A conditional tissue-specific transgene expression system using inducible GAL4. *Proceedings of the National Academy of Sciences of the United States of America* 98(22):12596-12601.
14. Roman G, Endo K, Zong L, & Davis RL (2001) P[Switch], a system for spatial and temporal control of gene expression in Drosophila melanogaster. *Proceedings of the National Academy of Sciences of the United States of America* 98(22):12602-12607.
15. Basler K & Struhl G (1994) Compartment boundaries and the control of Drosophila limb pattern by hedgehog protein. *Nature* 368(6468):208-214.
16. Jenett A, *et al.* (2012) A GAL4-driver line resource for Drosophila neurobiology. *Cell reports* 2(4):991-1001.
17. Kvon EZ, *et al.* (2014) Genome-scale functional characterization of Drosophila developmental enhancers in vivo. *Nature* 512(7512):91-95.
18. Fischbach KF & Dittrich APM (1989) The Optic Lobe of Drosophila-Melanogaster .1. A Golgi Analysis of Wild-Type Structure. *Cell Tissue Res* 258(3):441-475.
19. Morante J & Desplan C (2008) The color-vision circuit in the medulla of Drosophila. *Current biology : CB* 18(8):553-565.
20. Raghu SV & Borst A (2011) Candidate Glutamatergic Neurons in the Visual System of Drosophila. *Plos One* 6(5).
21. Wagh DA, *et al.* (2006) Bruchpilot, a protein with homology to ELKS/CAST, is required for structural integrity and function of synaptic active zones in Drosophila. *Neuron* 49(6):833-844.
22. Zipursky SL, Venkatesh TR, Teplow DB, & Benzer S (1984) Neuronal Development in the Drosophila Retina - Monoclonal-Antibodies as Molecular Probes. *Cell* 36(1):15-26.
23. Murphy S, *et al.* (2014) The Janelia Workstation for Neuroscience. *Keystone Big Data in Biology, San Francisco, CA*.
24. Peng HC, *et al.* (2011) BrainAligner: 3D registration atlases of Drosophila brains. *Nature methods* 8(6):493-U486.
25. Aso Y, *et al.* (2014) The neuronal architecture of the mushroom body provides a logic for associative learning. *eLife* 3.
26. Peng HC, Ruan ZC, Long FH, Simpson JH, & Myers EW (2010) V3D enables real-time 3D visualization and quantitative analysis of large-scale biological image data sets. *Nat Biotechnol* 28(4):348-U375.
27. Selleck SB & Steller H (1991) The influence of retinal innervation on neurogenesis in the first optic ganglion of Drosophila. *Neuron* 6(1):83-99.
28. Jefferis GSXE, *et al.* (2007) Comprehensive maps of Drosophila higher offactory centers: Spatially segregated fruit and pheromone representation. *Cell* 128(6):1187-1203.
29. Chou YH, *et al.* (2010) Diversity and wiring variability of olfactory local interneurons in the Drosophila antennal lobe. *Nat Neurosci* 13(4):439-U460.
30. Lin HV, Rogulja A, & Cadigan KM (2004) Wingless eliminates ommatidia from the edge of the developing eye through activation of apoptosis. *Development* 131(10):2409-2418.
31. Wolff T & Ready DF (1991) Cell death in normal and rough eye mutants of Drosophila. *Development* 113(3):825-839.

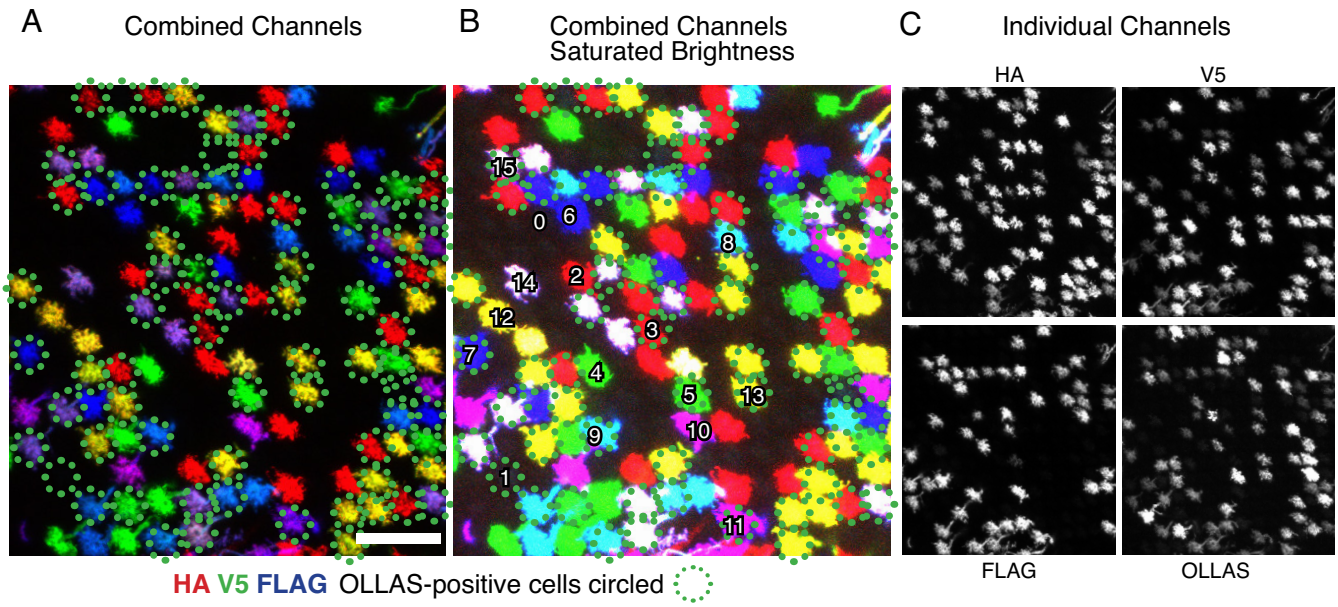

Fig. S1. MCFO labeling with four stop-cassettes (HA, V5, FLAG and OLLAS). Stop-cassette excision was induced by temperature-mediated FLP-induction as in Fig. 1 (30 min at 37°C). (A,B) All predicted 15 color combinations (plus the absence of labeling) were observed. Three markers (HA, V5 and FLAG) are shown as RGB images with the fourth label (OLLAS) indicated by dotted green circles. Numbers indicate examples of different marker combinations (even numbers [plus zero for absence of labeling] mark examples of combinations without OLLAS; the following odd numbers indicate the corresponding OLLAS positive combinations). Images show cross-section views of the array of terminals of T1-neurons in layer M2 of the medulla. In addition to the absence or presence of each marker, some differences in the expression level of each label between different T1-cells were also observed. Basic color combinations are therefore most easily seen with appropriately adjusted brightness (compare A and B). Individual channels of (A) are shown as grey scale images in (C). Scale bar, 20 µm.

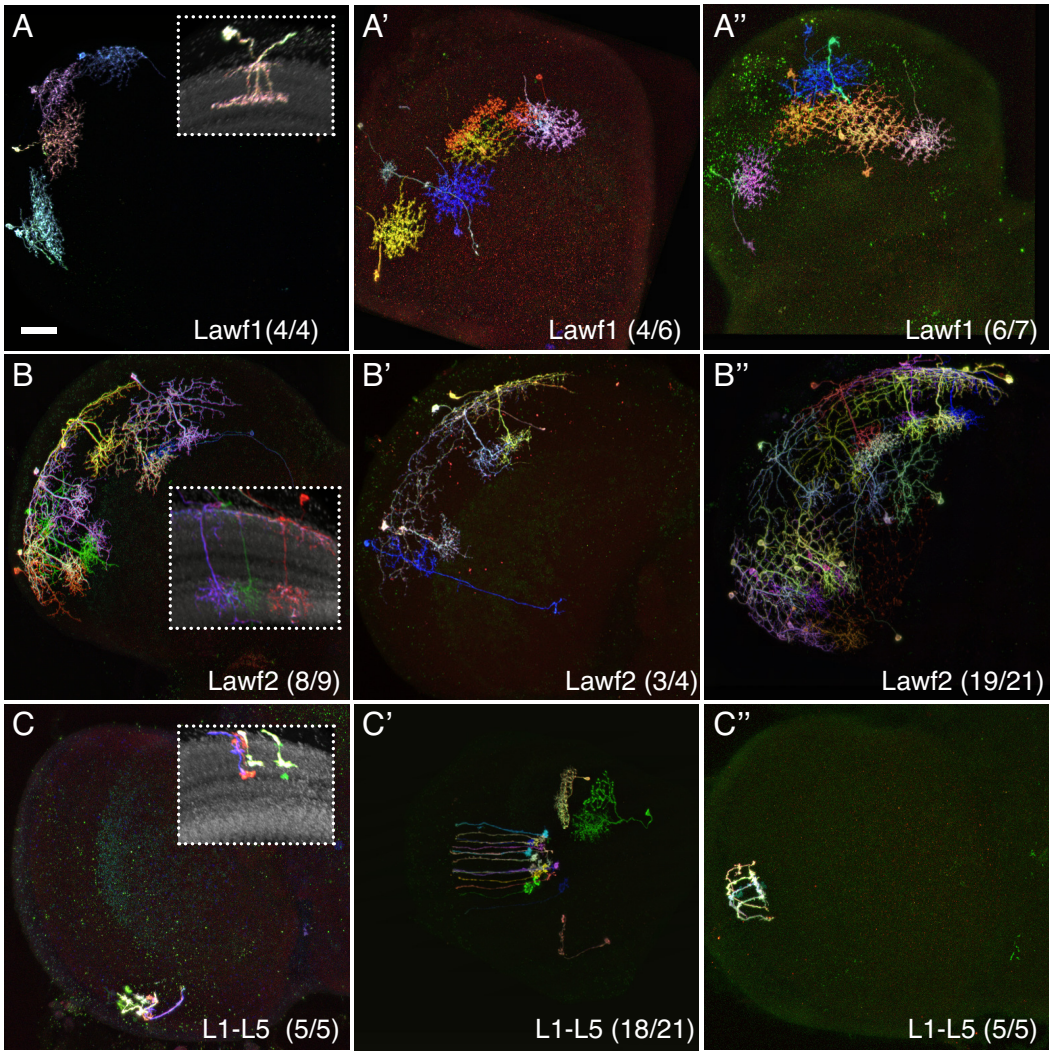

Fig. S2. Two-recombinase MCFO experiments can reveal common developmental origins of neurons. Examples of repeated co-labeling of multiple neurons of the same cell type or specific groups of cell types are shown. Images are all from experiments identical to those in Fig. 3F,G,G', showing flies with identical genotype and Flp-induction. Although labeling is not necessarily limited to the progeny of a single precursor cell per experiment, repeated co-labeling of specific groups of neurons as in these examples is difficult to explain without postulating a clonal relationship. Co-labeling of Lawf1 (A,A',A''), Lawf2 (B,B',B'') or lamina monopolar (L1-L5) (C,C'C'') cells. Images are maximum intensity projections through the entire optic lobe. Insets in (A,B,C) show reoriented views generated from the corresponding confocal stack to illustrate the identification of the labeled cell types. Numbers of labeled cells of the indicated cell types / total labeled cells are listed for each sample. Lamina monopolar (L1-L5) cells are known to derive from common precursors that differ from those of medulla neurons (27). Scale bar, 20 µm.

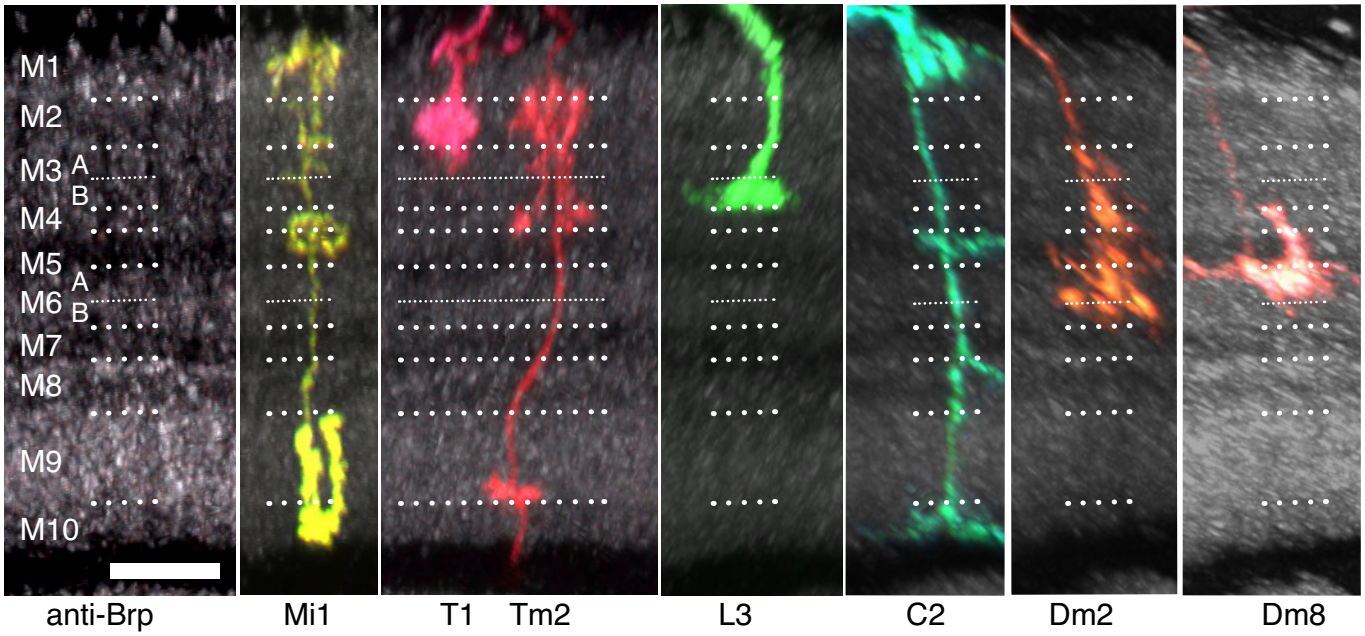

Fig. S3. Banding pattern of the anti-Brp (21) reference marker provides landmarks for medulla layer identification. Correspondence between alternating anti-Brp bands and layer designations used in Golgi studies (18) can be established by examination of known medulla cell types; M1, T1, Tm2, L3, C2, Dm2 and Dm8 are shown. In many cases, layers could be further subdivided based on position of specific neuronal types (also see Fig. S5). For example, M6A and M6B are defined by the different proximal terminations of Dm2 and Dm8 (right two panels). Single cell labeling was as in Fig. 3F,G,G′. Reoriented substack projections are shown. The anti-Brp pattern also provides a reference for computational alignment of different samples (24, 28). Scale bar represents 10 µm.

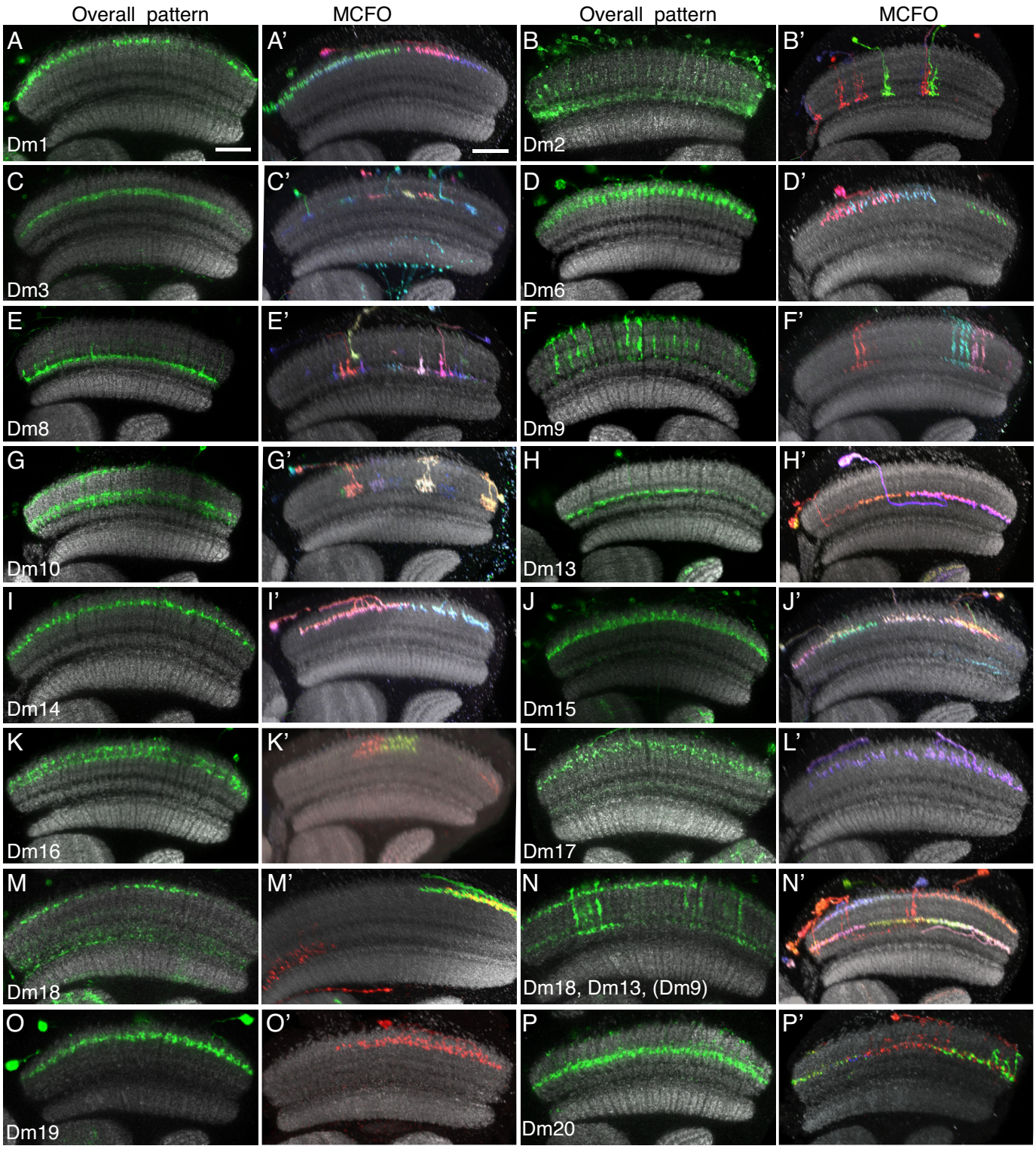

Fig. S4. Overall expression patterns and MCFO labeling of GAL4-driver lines for the Dm cell types that were only shown as schematics in Fig. 4. Cell types are indicated. GAL4 lines are listed in Table S3. Scale bars represent 20 μm.

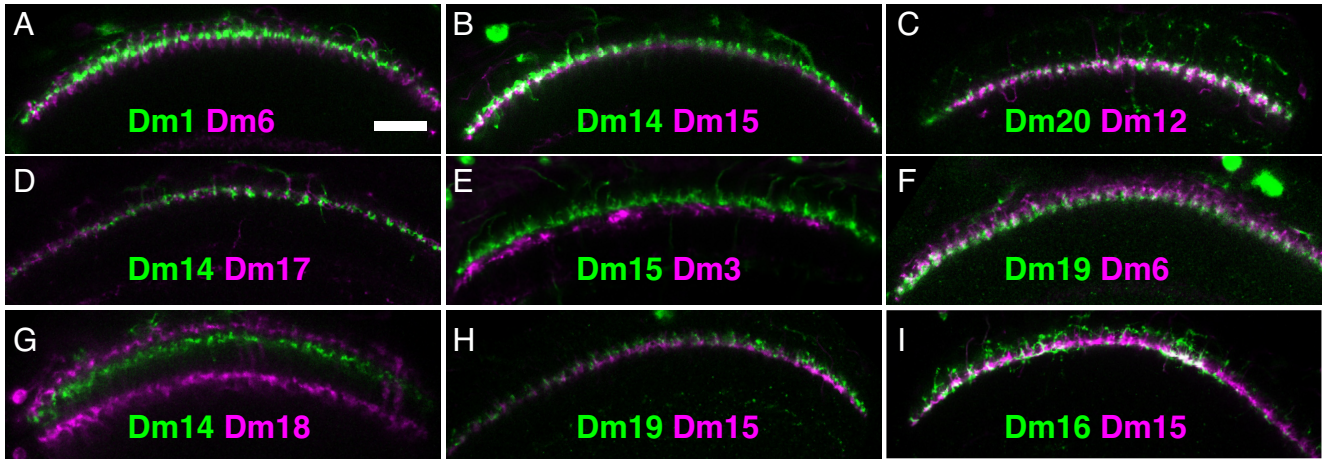

Fig. S5. Double labeling of Dm cell types using LexA and GAL4 driver lines reveals relative layer positions. Subtle but stereotyped differences in sublayer positions indicate cell-type differences in arbor stratification beyond the major layers and sublayers illustrated in Fig. S3. GAL4 (green) and LexA (magenta) driver lines used in each panel are listed in Table S3. Cell types are as indicated. Scale bar, 20 µm. (A) Dm1 and Dm6 overlap near the M1/M2 boundary but only Dm6 processes extend also into M2. (B) Dm14 and Dm15 overlap in a sublayer of M2 with Dm15 processes found very slightly more proximal. (C) The main arborization of Dm20 and Dm12 both occupy the proximal M3 layer. (D) Dm14 and Dm17 are found in the same M2 sublayer. (E) Dm15 processes (in M2) have a more distal position than those of Dm3 (in the distal M3 layer). (F) Dm19 and Dm6 overlap in M2 with Dm6 processes also found more distal (where they overlap with Dm1, see (A)). (G) Dm18 processes have a more distal location than those of Dm14 (in M2). The LexA line used also labels Dm13 (in ~ M4). (H) Dm19 and Dm15 overlap in a sublayer of M2 with Dm15 processes found very slightly more proximal. In combination with (B) this also confirms the matching layer positions of Dm14 and Dm19. (I) Dm15 and the more proximal Dm16 arbors overlap. Dm16 processes appear to extend very slightly more proximal.

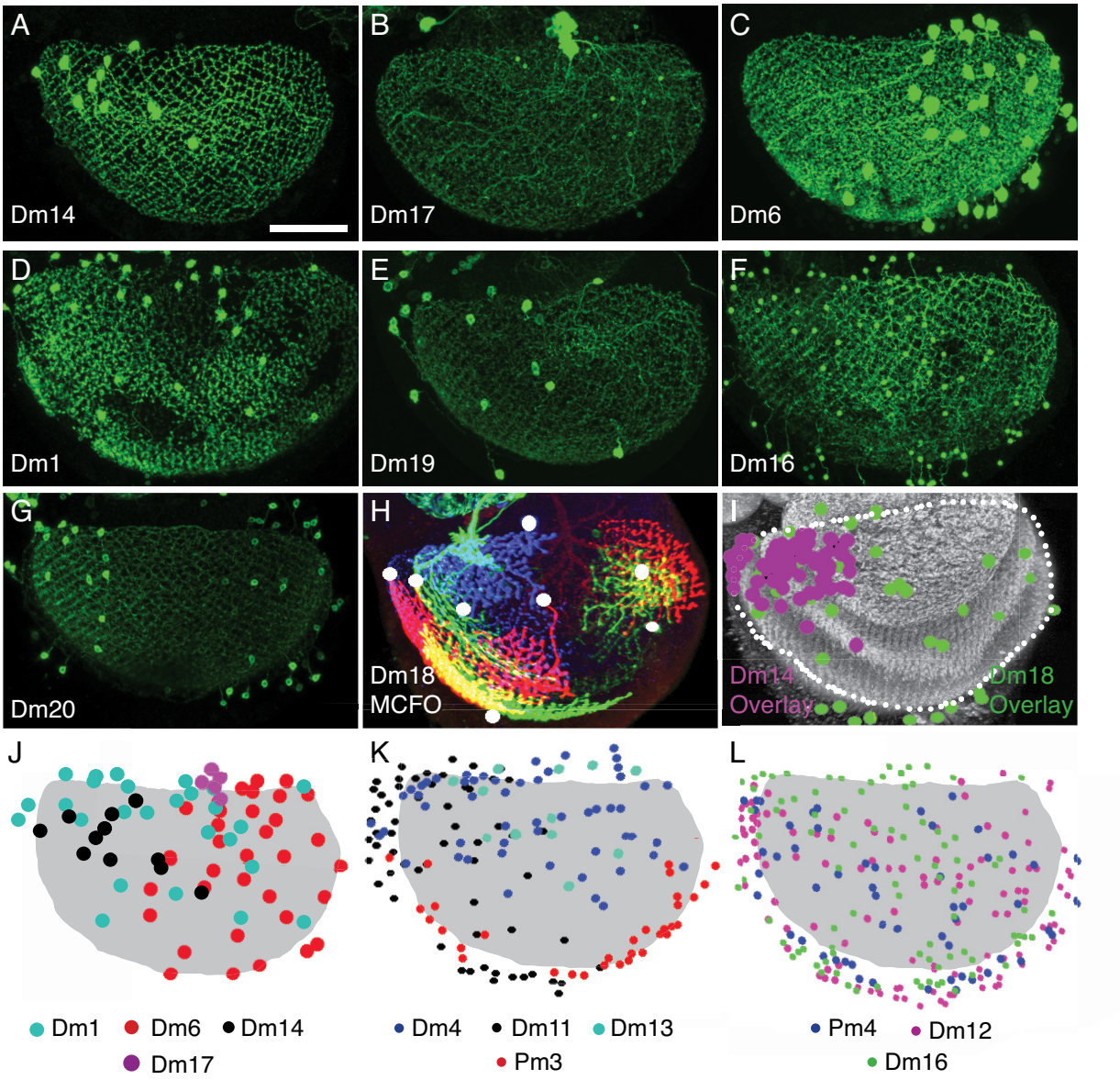

Fig. S6. Patterns of cell body distribution in the medulla cell body rind are cell type-specific. (A-G) Cell body distributions of selected Dm neurons. The arbors of Dm1, Dm6, Dm14, Dm16, Dm17 and Dm19 have similar layer positions in or near M2 (see Figs. 4, S4) but diverse cell body distributions. Dm20 (with processes mainly in layer M3) was the only Dm cell type which appears to have somata distributed preferentially in two non-overlapping regions (dorsal and ventral medulla cell body rind, similar pattern in n=4 optic lobes from two brains). Images are from the Janelia FlyLight collection and were generated as described (16). Anterior is up, dorsal left. Scale bar represents 20 µm. Although some lines do not label all cells of the cell type of interest (e.g. some Dm1 cells in (D) appear to be absent), these missing cells do not appear to be distributed in a specific pattern. (H,I) Cell body distributions can be obtained from multiple MCFO labeled specimens. (H) Image of an optic lobe with MCFO labeled Dm18 cells and other neurons. The GAL4 line used was VT028450. Dm18 cells were identified by shape and layer position using the full confocal stack and their cell body positions marked by the white circles in the projection image as shown. (I) Combined distributions of Dm18 and Dm14 cells from several aligned fly brains with MCFO labeling as illustrated in (H). Image shows 71 Dm14 cells from 14 optic lobes and 38 Dm18 cells from 11 optic lobes. The optic lobes used for this overlay were all aligned to the same template brain using the anti-Brp reference pattern (see SI Methods). The Anti-Brp pattern of the reference brain is shown in grey; the white dotted line marks the boundary of the medulla neuropil. The Dm14 distribution shows this method can produce similar patterns to those from single brains with specific labeling (A). Compared to Dm14, Dm18 cells have a wider distribution that also includes the ventral and posterior medulla cell body rind. (J) Schematic summarizing the positions of the somata of four M1/M2 layer Dm cell types: Dm1, Dm6, Dm14 and Dm17. Each cell type has a distinct stereotyped general distribution (for example, ventral for Dm6 and dorsal-anterior for Dm14) but the precise positions of individual cells varied between different optic lobes. Cell body size and approximate distance of the cell body from the neuropil also appear to be cell type inherent properties. (K) Schematic of additional examples of non-uniform cell body distributions. (L) Examples of cell types without strong regionalization of somata positions (schematic). For further description of Pm3 and Pm4, the two inner medulla cell types that are included in (K,L), see Fig. S8. Cell body distributions of all Dm neurons are summarized in Table S4.

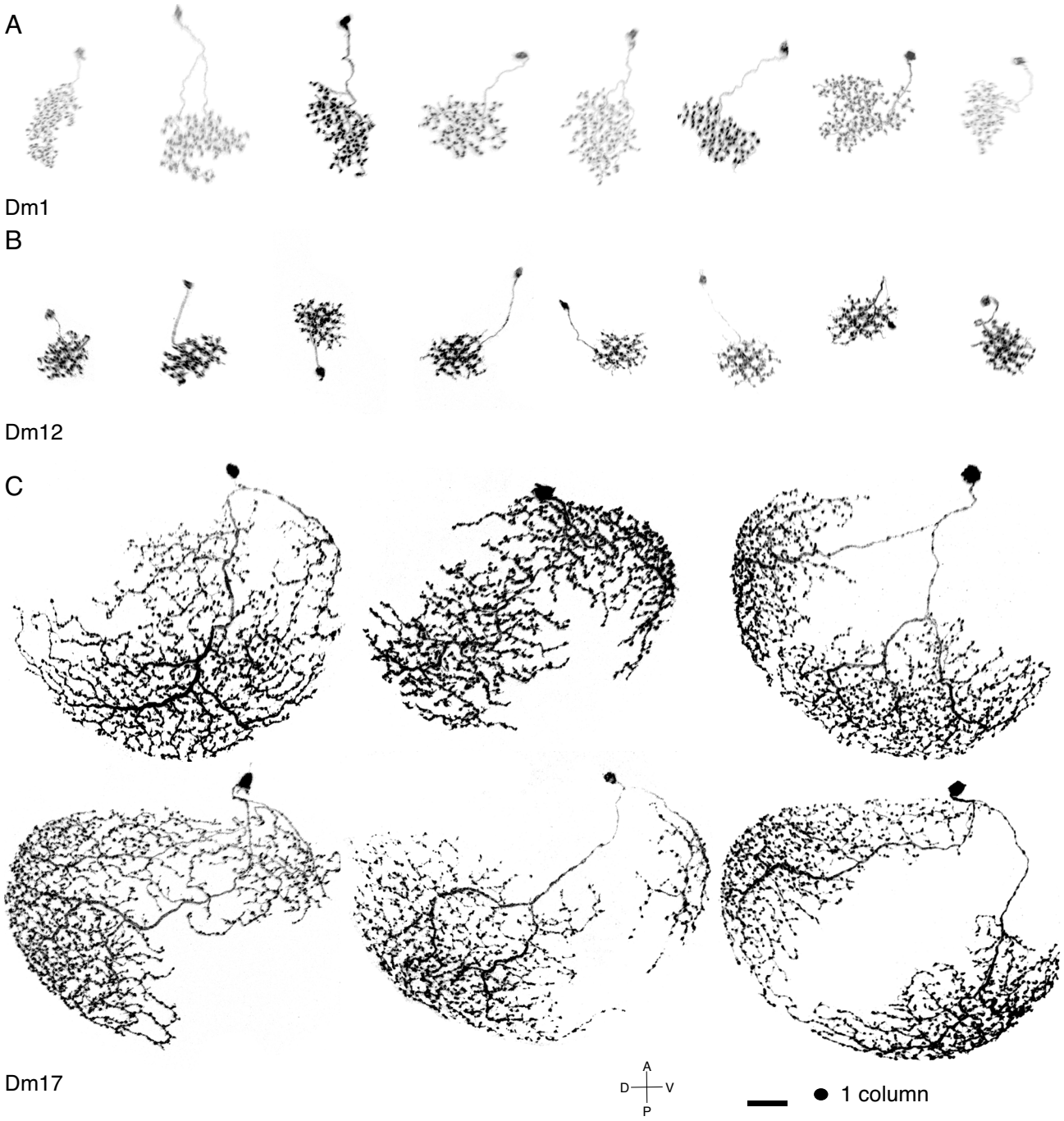

Fig.S7. Side by side comparison of layer cross-section views of multiple cells of each of three different Dm neuron types illustrates stereotypy and variability of arbor size and shape within layers. (A) Dm1. Eight segmented cells from 4 different optic lobes are shown. The precise shape of the area covered by each Dm1 cell is clearly different. (B) Dm12. Eight cells from 3 optic lobes. Dm12 arbors shape appears much less variable than Dm1. Dm1 cells are also generally slightly larger than Dm12 cells. (C) Dm17. Six cells from five optic lobes. Similar to Dm1, the overall shapes of Dm17 cells are highly variable. All Dm17 cells are much larger than Dm1 and Dm12 cells. Cells are shown at the same scale and orientation. Scale bar, 20 μm.

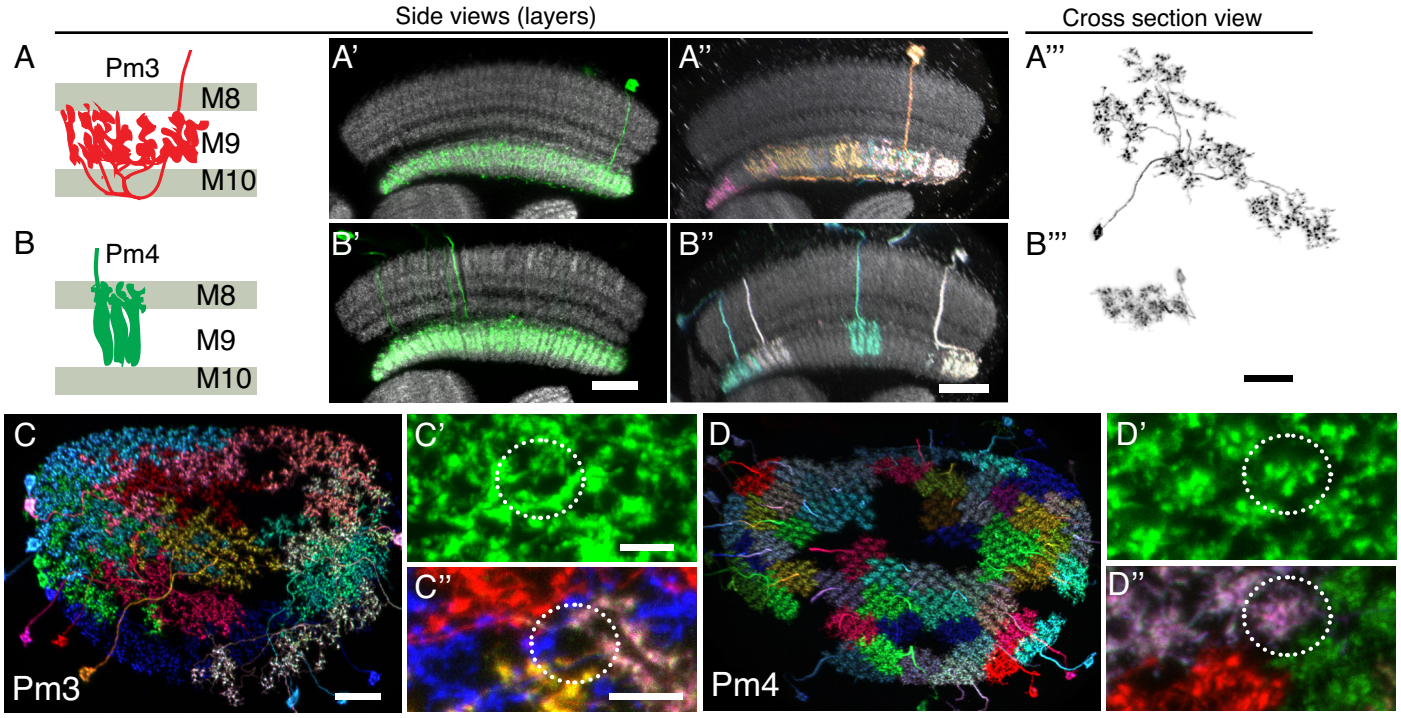

Fig.S8. Anatomy of Pm3 and Pm4 cell types. (A,B) Schematic of side views of individual cells to illustrate layer position, (A',B') GAL4 line pattern, (A'',B'') GAL4-line MCFO and (A''',B''') cross-section views of individual cells (compare to Fig. 5A). Images were generated and displayed as for Figs. 4 and 5. Scale bar, 20 µm. (C-C'',D-D'') Coverage patterns of Pm3 and Pm4 cells (compare Fig. 6). Distribution of MCFO labeled cells across the entire medulla (C,D), and higher magnification views of the full GAL4 pattern (C',D') and MCFO labeled processes (C'',D'') are shown as in Fig. 6. White dashed circles indicate the approximate size of a medulla column. (C,C',C'') Pm3. Pm3 neurons display a striking intermingling of processes of different cells; the non-uniform distribution of the arbor density of individual Pm3 cells across medulla columns (also see A''') is reminiscent of a group of highly variable local interneurons in the fly antennal lobe (29). (D,D',D'') Pm4. Pm4 cells show a tiling pattern similar to Dm4. Scale bars, 20 µm (A'-A''',B'-B''',C,D), 5 µm for (C',C'',D',D'').

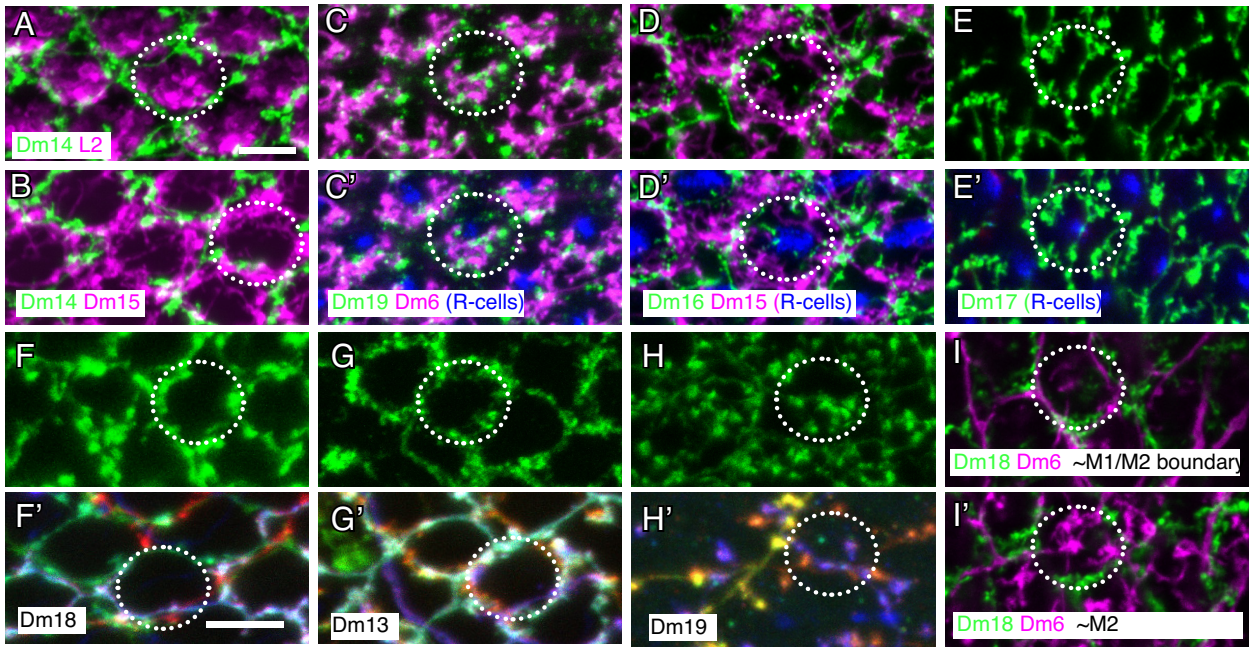

Fig. S9. Intracolumnar positions of Dm neurons with arbors in or near layer M2. (A) Peripheral column position of Dm14 processes relative to L2 lamina neuron terminals and (B) similar positions of Dm14 and Dm15 as revealed by LexA/GAL4 double labeling. Images show processes in layer M2. (C,C′) Co-labeling of Dm6 and Dm19 in M2 shows majority of processes of both cell types in a central column position (similar to that of L2 terminals). (C′) shows same image as (C) but with photoreceptor (R-cell) axons in blue as an additional landmark. (D,D′) Dm15 and Dm16 processes in the proximal part of M2 both have peripheral column positions. Lower panel (D′) includes R-cells. (E,E′) Dm17 arbors (shown alone or together with R-cells) do not show an obvious preference for a specific column region. (F,F′-H,H′) Similar arbor distributions of different cell types in different layers and distinct distributions of similar cells in the same layer. Overall GAL4 line patterns and MCFO images of Dm18, Dm13 and Dm19 processes shown as in Fig.6. Note the similarity of Dm18 (F,F′; processes near M1/M2 boundary) and Dm13 (G,G′; processes in M4) to Dm14 (Fig. 6G′,G″; processes in M2). By contrast, Dm19 (in the same M2 sublayer as Dm14) shows a pattern clearly distinct from Dm14. (I,I′) Intracolumnar positions can differ between sublayers. (I) Dm6 neurites at the M1/M2 boundary are found in the column periphery near Dm18 processes. By contrast, slightly deeper in the medulla in layer M2, Dm6 terminals occupy a central column position (I′, also C,C′). Scale bars, 5 µm. Bar in (F′) applies to DPX-mounted samples in (F′,G′,H′). LexA and GAL4 driver lines are listed in Table S3.

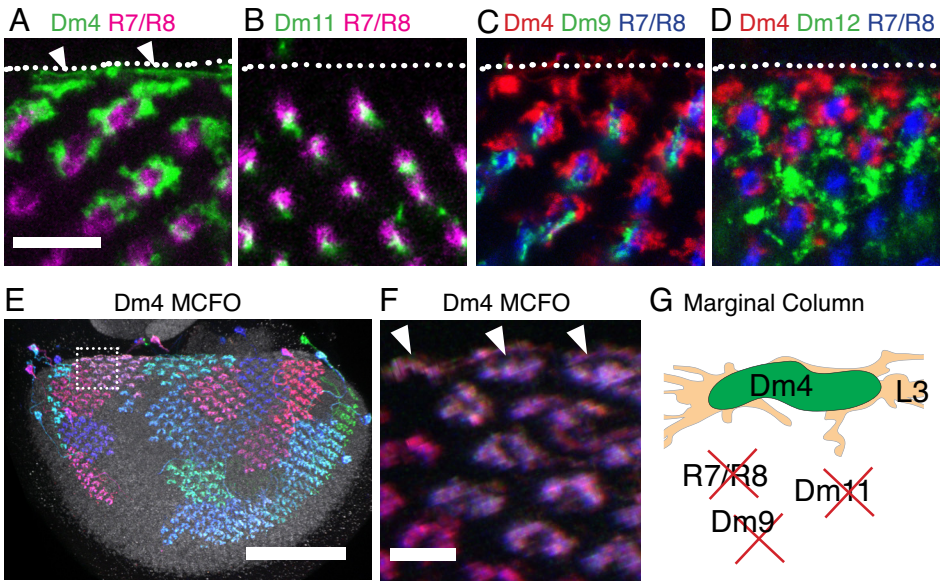

Fig. S10. Altered cellular composition and structure of marginal medulla columns. (A) Dm4 and R7/R8 cells in columns at and near the anterior margin of the medulla. Marginal columns (upper portion of panel) lack R7/R8 in adult flies due to pupal apoptosis of R-cells in incomplete ommatidia (30, 31) but contain Dm4 arbors. Dm4 terminals within these columns have a more elongated shape (arrowheads). White dotted lines in (A-D) indicate the approximate position of the edge of the medulla neuropil. (B,C,D) The R7/R8 associated processes of Dm11 (B) and Dm9 (C) are absent from marginal columns whereas processes of Dm12 cells extend into these columns (D). (C) and (D) also show Dm4 cells. Some gaps in the Dm9 (and also Dm4) pattern, indicating unlabeled cells, were observed in these experiments but this stochastic expression does not account for the consistent absence of Dm9 from marginal columns. (E,F) MCFO labeling shows individual Dm4 cells at the medulla margin span both marginal and other columns. Shape differences are therefore local changes that affect only part of the arbors of each marginal Dm4 cell. (E) Overview of medulla with Dm4 MCFO and anti-Brp reference marker in grey. (F) Detailed view of the area boxed in (E). Arrowheads indicated marginal columns. (G) Schematic of cellular structure of marginal columns in medulla layer M3; compare to the schematic shown in Fig. 8I. Only those cell types shown in Fig. 8I are included. Dm4 and L3 are present but with altered shapes and Dm9 and Dm11 are missing. No obvious differences were observed for Dm12, which is not included in the schematic. Scale bars, 10 µm (A-D), 50 µm (C), 5 µm (D).

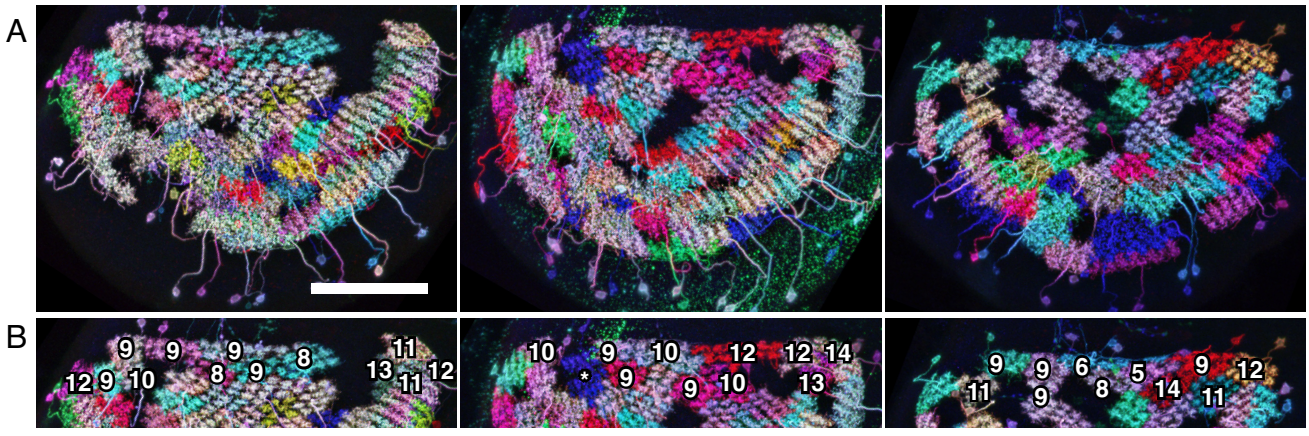

Fig. S11. Details of tiling arrangements are not stereotyped. (A) Three examples of the distribution of Pm4 cells in the medulla. To illustrate that the patterns do not match precisely, cell size (in columns) is indicated for cells near the anterior margin (used as a landmark) in (B). Asterisk indicates a pair of cells that could not be counted separately. Images are maximum intensity projections. Quantification was done on the corresponding confocal stacks. Scale bar, 50 µm.

Table S1 Transgene constructs

Name	Codon Usage	Insertion
pJFRC46-8XLexAop2-Syt::smGFP-OLLAS	Drosophila	attP18
pJFRC47-8XLexAop2-Syt::smGFP-HA	Drosophila	su(Hw)attP1
pJFRC51-3XUAS-IVS-Syt::smGFP-HA	Drosophila	su(Hw)attP1
pJFRC120-5XUAS-DenMark::smGFP-V5	Drosophila	su(Hw)attP5
pJFRC121-3XUAS-DenMark::smGFP-v5	Drosophila	su(Hw)attP5
pJFRC122-5XUAS-IVS-Syt::smGFP-HA	Drosophila	VK00005
pJFRC123-3XUAS-IVS-Syt::smGFP-V5	Drosophila	VK00005
pJFRC135-3XUAS-IVS-Flp2	yeast	attP40
pJFRC136-5XUAS-IVS-Flp2	yeast	attP40
pJFRC137-1XUAS-IVS-FlpL2	yeast	attP40
pJFRC138-3XUAS-IVS-FlpL2	yeast	attP40
pJFRC139-3XUAS-IVS-FlpL	yeast	attP40
pJFRC140-1XUAS-DSCP-FlpL2	yeast	attP40
pJFRC141-3XUAS-DSCP-FlpL2	yeast	attP40
pJFRC144-1XUAS-IVS-Flp2-Rs	R. sphaeroides	attP40
pJFRC145-3XUAS-IVS-Flp2-Rs	R. sphaeroides	attP40
pJFRC146-5XUAS-IVS-Flp2-Rs	R. sphaeroides	attP40
pJFRC147-1XUAS-IVS-Flp2-At	A. thaliana	attP40
pJFRC148-3XUAS-IVS-Flp2-At	A. thaliana	attP40
pJFRC149-5XUAS-IVS-Flp2-At	A. thaliana	attP40
pJFRC199-5XUAS-IVS-myr::smGFP-HA	Drosophila	VK00005
pJFRC200-10XUAS-IVS-myr::smGFP-HA	Drosophila	attP18,attP2
pJFRC201-10XUAS-FRT>STOP>FRT-myr::smGFP-HA	Drosophila	VK00005, attP40
pJFRC202-10XUAS-IVS-myr::smGFP-cMyc	Drosophila	attP2
pJFRC203-10XUAS-FRT>STOP>FRT-myr::smGFP-cMyc	Drosophila	attP40
pJFRC204-5XUAS-IVS-myr::smGFP-V5	Drosophila	VK00005
pJFRC205-10XUAS-IVS-myr::smGFP-V5	Drosophila	attP18, attP2
pJFRC206-10XUAS-FRT>STOP>FRT-myr::smGFP-V5	Drosophila	attP40
pJFRC207-10XUAS-IVS-myr::smGFP-FLAG	Drosophila	attP2
pJFRC208-10XUAS-FRT>STOP>FRT-myr::smGFP-FLAG	Drosophila	attP40
pJFRC209-10XUAS-IVS-myr::smGFP-OLLAS	Drosophila	attP2
pJFRC210-10XUAS-FRT>STOP>FRT-myr::smGFP-OLLAS	Drosophila	attP2
pJFRC213-13XLexAop2-IVS-myr::smGFP-HA	Drosophila	su(Hw)attP1
pJFRC214-13XLexAop2-KDRT>-dSTOP-KDRT>-myr::smGFP-HA	Drosophila	VK00005
pJFRC215-13XLexAop2-FRT>-dSTOP-FRT>-myr::smGFP-HA	Drosophila	VK00005
pJFRC216-13XLexAop2-IVS-myr::smGFP-V5	Drosophila	su(Hw)attP8
pJFRC217-13XLexAop2-KDRT>-dSTOP-KDRT>-myr::smGFP-V5	Drosophila	su(Hw)attP1
pJFRC218-13XLexAop2-FRT>-dSTOP-FRT>-myr::smGFP-V5	Drosophila	attP40
pJFRC219-13XLexAop2-IVS-myr::smGFP-FLAG	Drosophila	su(Hw)attP8
pJFRC220-13XLexAop2-KDRT>-dSTOP-KDRT>-myr::smGFP-FLAG	Drosophila	su(Hw)attP5
pJFRC221-13XLexAop2-FRT>-dSTOP-FRT>-myr::smGFP-FLAG	Drosophila	su(Hw)attP2
pJFRC222-13XLexAop2-IVS-myr::smGFP-OLLAS	Drosophila	attP18
pJFRC223-13XLexAop2-FRT>-dSTOP-FRT>-myr::smGFP-OLLAS	Drosophila	attP2
pJFRC224-13XLexAop2-KDRT>-dSTOP-KDRT>-myr::smGFP-OLLAS	Drosophila	attP2
pJFRC225-5XUAS-IVS-myr::smGFP-FLAG	Drosophila	VK00005
pJFRC226-10XUAS-KDRT>-dSTOP-KDRT>-myr::smGFP-HA	Drosophila	VK00005
pJFRC227-10XUAS-KDRT>-dSTOP-KDRT>-myr::smGFP-OLLAS	Drosophila	attP2
pJFRC228-10XUAS-KDRT>-dSTOP-KDRT>-myr::smGFP-V5	Drosophila	su(Hw)attP1
pJFRC229-10XUAS-B3RT>dSTOP-B3RT>-myr::smGFP-FLAG	Drosophila	su(Hw)attP6
pJFRC230-10XUAS-B3RT>dSTOP-B3RT>-myr::smGFP-HA	Drosophila	VK00005
pJFRC231-10XUAS-B3RT>dSTOP-B3RT>-myr::smGFP-OLLAS	Drosophila	attP2
pJFRC232-10XUAS-B3RT>-dSTOP-B3RT>-myr::smGFP-V5	Drosophila	su(Hw)attP5, su(Hw)attP1
pJFRC239-10XUAS-FRT>STOP>FRT-myr::smGFP-V5-THS-10XUAS-FRT>STOP>FRT-myr::smGFP-cMyc	Drosophila	su(Hw)attP5, su(Hw)attP1
pJFRC240-10XUAS-FRT>STOP>FRT-myr::smGFP-V5-THS-10XUAS-FRT>STOP>FRT-myr::smGFP-FLAG	Drosophila	su(Hw)attP5, su(Hw)attP1
pJFRC241-10XUAS-FRT>STOP>FRT-myr::smGFP-FLAG-THS-10XUAS-FRT>STOP>FRT-myr::smGFP-cMyc	Drosophila	su(Hw)attP5, su(Hw)attP1
pJFRC242-10XUAS-IVS-myr::sfGFP-THS-10XUAS-FRT>STOP>FRT-myr::smGFP-HA	Drosophila	attP40,attP2
R57C10-Flp2	yeast	attP18, su(Hw)attP8
R57C10-Flp2::PEST	yeast	attP18, su(Hw)attP8
R57C10-FlpL	yeast	su(Hw)attP8
R57C10-FlpL2	yeast	su(Hw)attP8
pBPhsFlp2::PEST	Drosophila	attP3
29C07-KDGeneswitch-4		attP40
tubP-FRT>GAL80-6-FRT>		VK00027
tubP-B3RT>GAL80-6-B3RT>		VK00027
tubP-KDRT>GAL80-6-KDRT>		VK00027

Table S2 Fly lines with combinations of transgenes

Short Name	Genotype	Figures
HA_V5	pJFRC200-10XUAS-IVS-myr::smGFP-HA in attP18 , pJFRC216-13XLexAop2-IVS-myr::smGFP-V5 in su(Hw)attP8 (both on the x-chromosome)	1E,E';4A,B,C;6A'-I';8D,H;S4A-P; S5; S8A',B',C',D';S9A,B,C,C'-E,E',F-I,I';S10A-D
HA_V5_FLAG	pJFRC201-10XUAS-FRT>STOP>FRT-myr::smGFP-HA in VK0005, pJFRC240-10XUAS-FRT>STOP>FRT-myr::smGFP-V5-THS-10XUAS-FRT>STOP>FRT-myr::smGFP-FLAG in su(Hw)attP1 (all on chromsome 3)	see combined stocks below
HA_V5_FLAG_OLLAS	HA_V5_FLAG plus pJFRC210-10XUAS-FRT>STOP>FRT-myr::smGFP-OLLAS in attP2 (all on chromsome 3)	see combined stocks below
MCFO-1	pBPhsFlp2::PEST in attP3;; HA_V5_FLAG	1F,F',G,G';2;3G,G';4A',A'',B',B'',C',C''; 5A (all except Dm17,Dm19),B-E; 6A,A'',B,B'',C',C'',D',D'',E',E'',F',F'',G'',H', H'';7B,B'-F,F';8E,F,G; 9A-D;S2;S3; S4A',C'-G',I',J'; S7A,B; S8A'',B'',C,C'',D,D''; S9H'; S10E,F; S11
MCFO-2	pBPhsFlp2::PEST in attP3;; HA_V5_FLAG_OLLAS	S1
MCFO-3	R57C10-FlpL in su(Hw)attP8;; HA_V5_FLAG	3C
MCFO-4	R57C10-Flp2 in su(Hw)attP8;;HA_V5_FLAG	3B;S4M';S6H,I
MCFO-5	R57C10-Flp2::PEST in in su(Hw)attP8;; HA_V5_FLAG	3A
MCFO-6	R57C10-FlpL in su(Hw)attP8;;HA_V5_FLAG_OLLAS	6G;7A,A';S4B',N'; S9F',G'
MCFO-7	R57C10-Flp2::PEST in in attP18;;HA_V5_FLAG_OLLAS	5A (Dm17,Dm19);6I,I'; 8A,B,C; S4H',K',L',O',P'; S7C
	OL-KD (29C07-KDGeneswitch-4) in attP40; R57C10-GAL4 in attP2 tubP-KDRT>GAL80-6-KDRT> in VK00027	3G,G';4A'',B'',C'';5A (all except Dm14,Dm17,Dm19,Dm20);S2;S3
	pJFRC137-1XUAS-IVS-FlpL2 in attP40; R57C10-GAL4 in attP2	3E

Table S3 GAL4, split-GAL4 and LexA driver lines

Cell type*	Driver Line	Insertion site (s)	Figures
Dm1	R22D12-GAL4	attP2	6E,E',E";S4A,A'; S5A; S6D;S7A
	R22D12-LexAp65	attP40	
Dm2	R26H07-GAL4	attP2	7A,7A';S4B,B'
Dm3	R20D11-GAL4	attP2	5B;S4C,C'
	R20D11-LexAp65	attP40	S5E
Dm4	R23G11-GAL4	attP2	4B,B';6A,A',A";7E,E'; 9D;S10E,F
	R23G11-LexA	attP40	S10A,C,D
Dm6	R38H06-GAL4	attP2	6D,D',D";S4D,D';S6C
	R38H06-LexAp65	attP40	S5A,F;S9C,C',I,I'
Dm8	R24F06-GAL4	attP2	6C,C',C";7C,C';S4E,E'
	R24F06-LexAp65	attP40	
Dm9	R42H01-GAL4	attP2	8H;9A; S4F,F'; S10C
	R42H01-LexAp65	attP40	
Dm10	R30B06-GAL4	attP2	7B,B';S4G,G'
Dm11	R11C05-GAL4	attP2	4A,A';6B,B";7F,7F';9B
	R11C05-nlsLexAGADfl	attP40	6B';8H;S10B
Dm12	R47G08-GAL4	attP2	4C,C';5E;6F,F',F"; S7B; S10D
	R47G08-LexAp65	attP40	8D; S5C
Dm13	R38A07-GAL4	attP2	S4H,H';S9G
Dm14	R47E05-GAL4	attP2	5A;6G,G',G";S4I,I';S5B,D,G; S6A,I;S9A,B
Dm15	R18G08-GAL4	attP2	5D;S4J,J';S5E
	R18G08-LexAp65	attP40	S5B,H,I; S9B,D,D'
Dm16	R58G11-GAL4	attP2	5C;S4K,K';S5I; S6F;S9D,D'
Dm17	VT043152-GAL4	attP2	S4L,L';6I,I',I";S6B; S7C;S9E,E'
	R58G03-GAL4	attP2	5A
	R23C03-LexAp65	attP40	S5D
Dm18, (Dm13)	VT028450-GAL4	attP2	S4M,M';S6H,I; S9F
Dm18, Dm13, (Dm9)	R60C01-GAL4	attP2	S4N,N';S9F',G',I,I'
	R60C01-LexAp65	attP2	S5G
Dm19	VT024602-GAL4	attP2	5A;S4O,O';S5F,H;S6E;S9C,C',H,H'
Dm20	VT049111-GAL4	attP2	5A;6H,H',H";8D;S4P,P';S5C;S6G
Pm3	R65D05-GAL4	attP2	S8A',A",C,C',C"
	R65D05-LexAp65	attP40	
Pm4	R53C05-GAL4	attP2	9C;S8B',B",D,D',D";S11
	R53C03-nlsLexAGADfl	attP40	
L2	R16H03-LexAp65	attP40	S9A
L3	R14B07-GAL4	attP2	1E,E',F,F',G,G';3A,B,C
	R22E09-nlsLexAGADfl	attP40	
T1	R31F10-p65ADZp; R30F10-ZpGdbd	attP40; attP2	2A,B,C;S1A,B,C
Dm9, Dm1	R19G04-p65ADZp; R53A05-ZpGdbd	attP40; attP2	7D,D'
C2,C3	R20C11-p65ADZp; R48D11-ZpGdbd	attP40; attP2	2D,E
Dm4, Dm9, Dm12	R15C05-GAL4	attP2	8A,B,C
L3, Dm4, Dm11	R75H07-GAL4	attP2	8E,F,G
Mature Neurons	R57C10-GAL4	attP2	3E,G,G';4A",B",C";5A (all except Dm14,Dm17,Dm19,Dm20); S2;S3

* All listed GAL4 and LexA lines are also expressed in several other cell populations but are sufficiently specific to serve as markers for the indicated Dm and Pm neuron types.

Table S4 Properties of Dm neuron cell types described in this study

Name	Layer pattern	Arbor size, shape and distribution within layers	Cell body distribution and estimated cell number	Notes	References
Dm1	**M1/M2 boundary** (in the same sublayer as Dm18; more proximal than the branches of Dm9 and Dm10 in M1)	Variable arbor shape; arbors cover ~ 20-30 columns; **distinct bouton-like terminals**; peripheral column position; areas covered by different cells overlap	Anterior part of medulla cell body rind (MCBR); ~40 cells per OL	Distinguished from Dm18 by smaller size and bouton-like terminals	(1), listed by name but not shown in (2)
Dm2	**M3 to M6B**	**Oriented arbors**: M6B arbors extend into neighboring columns on the dorsal side; **small** arbor spread (~ 2 columns in M6, 1 in other layers)	Throughout MCBR; large number of cells [not counted; the R26H07 GAL4 line also includes some Mi14 and Mi15 cells]; size and coverage pattern suggest ~ 1 cell per column	Shape and small size distinct	(1, 3), listed by name but not shown in (2)
Dm3	**M3A** (proximal to Dm15 processes in M2 and distal to Dm4, Dm12 and Dm20 in M3B)	**Distinct narrow elongated shape**: ~ 1 column wide and ~ 10 columns long; **arbors overlap considerably** (=high coverage); **oriented arbors**: cells are aligned with rows of medulla columns; most cells are extended in one of **two orthogonal orientations** (some cells show switches between rows or turns of direction)	Throughout MCBR; large number of cells [not counted; could be up to ~ one per column]	Oriented long narrow arbors distinct	(1, 2)
Dm4	**M3B and M5/M6 boundary** (Main neurite extends deeper into ~ M6 and turns back to arborize in M5/M6 and M3B)	Variable arbor shape; **arbors tile**, median column spread ~21 columns (see Fig. 9 for size distribution); central column position (surrounding R7/R8 axons); **cell boundaries follow column boundaries**	Anterior MCBR; ~ 40 cells per OL	Combination of terminal shape and tiling pattern distinct	(1, 2, 3)
Dm6	**M1/2 boundary and M2**; (layer position overlaps with both the Dm1/Dm18 and Dm14/Dm17/Dm19 sublayers)	Variable shape; **arbors overlap**; each column contains processes of several Dm6 cells; **intracolumnar position (~ matching L2 terminal) more central than that of, for example, Dm1 and Dm14** ; medium large cells (area covered ~ 30-40 columns)	Ventral ~two thirds of MCBR ; ~ 30 cells per OL	Distinguished from other M1/M2 layer Dm neurons by cell body distribution, central intracolumnar position (only Dm19 is similar), precise layer position and arbor size and structure	(1, 2)
Dm8	**M6A with recurrent processes into M4**	**Highest arbor density in center of cell with thinner radial processes extending laterally**; R7 associated dense center typically in single column with lateral arbors contacting > 10 columns; arbors overlap considerably (= high coverage) but centers of high arbor density approximately tile	Throughout MCBR ; large number of cells [not counted; could be up to ~ one per column]; coverage pattern consistent with nearly 1 cell per column	Arbor distribution in M6 (dense center and thinner lateral extensions) and recurrent M6 to M4 processes distinct	(1, 2, 3)
Dm9	**Distal M1 to M6A**	**Arbors overlap in M1 and M6A but otherwise tile**; processes in M2 to M5 occupy a central column position and are **closely associated with R7 and R8 photoreceptor axons;** median column spread in M2-M5 ~7 columns (see Fig. 9 for size distribution), slightly larger arbor spread in M1 and M6	Throughout MCBR; ~ 110 cells per OL	Tubular shape, tiling pattern and central column position around R-cell axons distinct Absent from medulla edge columns that lack R7/R8	(3), similar or identical to "glia-like Dm" (4)
Dm10	**Distal M1, M3B and M5**	**Arbor shape ~ ellipse** with long axis aligned with DV axis; small arbor spread (< 10 columns); arbors overlap; processes in peripheral (M1) or slightly peripheral (M3B,M5) intracolumnar position	Throughout MCBR; ~ 300 cells per OL	Distinct tri-stratified layer pattern	(3), similar or identical to "$Dm_{1,5}$" (2)
Dm11	**M1 to M6A (**the primary neurite extends beyond M6A and then turns back; recurrent processes from M6 to M1 and beyond M1 into the the first optic chiasm)	**Arbors tile**; median column spread ~9 columns (see Fig. 9 for size distribution); overall shape variable; **processes in M6A cover layer;** in other layers present as **thin processes [one per column] associated with R7 and R8 photoreceptor axons**	Dorsal MCBR; ~ 70 cells per OL	Tiling pattern in M1-M6 and extension of processes distally beyond medulla neuropile distinct R7/R8 associated processes absent from medulla edge columns (which lack R7/R8)	
Dm12	**M3B** (Main neurite extends into ~ M6 and turns back to project to M3B)	Arbors overlap; **roughly circular shape;** lateral spread ~ 15-20 columns; peripheral intracolumnar position	Throughout MCBR; ~ 120 cells per OL	Differs from Dm20 (also mainly in M3B) by size, arbor shape and cell body distribution	
Dm13	**M4** (primary neurite extends into deeper layers and turns back to form M4 branches)	Cells overlap ; **"gridlike" arbor arrangement similar to Dm14 and Dm18; peripheral intracolumnar position;** large cells (covered area ~ 50-100 columns)	Anterior MCBR ; ~ 15-20 cells per OL	Only monostratified Dm neuron in ~M4	
Dm14	**M2** (same sublayer position as Dm17 and Dm19; proximal to Dm1/Dm18)	Cells overlap; **"gridlike" arbor arrangement similar to Dm13 and Dm18; peripheral intracolumnar position** ; large cells (covered area ~ 50-100 columns)	Dorsal anterior MCBR; ~ 15 cells per OL	Regular "grid-like" pattern of processes in column periphery different from Dm17 and Dm19; smaller than Dm17 and Dm19; larger than Dm15	

Table S4 Properties of Dm neuron cell types described in this study (continued)

Name	Layer pattern	Arbor size, shape and distribution within layers	Cell body distribution and estimated cell number	Notes	References
Dm15	**M2** (arbors overlap with those of Dm14, Dm17 and Dm19 but appear to extend slighty deeper)	**Shape ~ ellipse** with longer axis of this ellipse typically **oriented at slight angle to anterior-posterior axis** of medulla; **small arbor size** (lateral spread < 10 columns); peripheral intracolumnar position, arbors overlap	Throughout MCBR ; ~ 250 cells per OL	Small size and ellipsoid arbor shape different from all other monostratified M1/M2 layer Dm neurons	
Dm16	Bistratified with main arbors near the **M1/ M2 and M2/M3 boundaries**	**Oriented arbors:** elongated along DV axis with higher arbor density at dorsal end of cell**;** peripheral column position	Throughout MCBR; ~ 100 cells per OL	Bistratified arborization in ~ M2 and asymmetric lateral process distribution unique	
Dm17	**M2** (same sublayer as Dm14 and Dm19)	**Very large cells** (covered area ~ 1/3 to over 1/2 of M2 layer); many cells have bifurcated main neurites and cover separate medulla regions; intracolumnar position of processes appears more variable than that of, for example, Dm14 or Dm6	~ 5 cells near the anterior edge of the medulla	Very large size and cell body position at anterior medulla margin characteristic; intracolumnar arbor distribution matches neither the central Dm19 nor the peripheral Dm14 pattern precisely	
Dm18	**M1/2 boundary** (same sublayer as Dm1)	**"Gridlike" arbor arrangement similar to Dm13 and Dm14**; large cells (covered area ~ 50-100 columns); **peripheral intracolumnar position**	Throughout MCBR; cell number estimated to be around ~ 20 per OL [lines include other cell types]	Differs from Dm1 by size (Dm18 arbors spread across more columns than those of Dm1) and the absence of prominent bouton-like terminals	
Dm19	**M2** (same sublayer as Dm14 and Dm17)	Variable shape; **large cells** (covered area ~ 100-200 columns; second largest Dm after Dm17); majority of **processes in central intracolumnar position similar to Dm6** but different from, for example, Dm14	Dorsal ~ two thirds of MCBR; ~ 15 cells per OL	Intracolumnar position different from Dm14 and, to a lesser extent, Dm17; Cell body distribution different from Dm17	
Dm20	**M3B** (some branches into more proximal and more distal layers; branches multiple times between edge of M1and M3B)	Variable arbor shape; **large cells** (covered area ~ 50-100 columns); **peripheral intracolumnar position** similar to Dm12 (i.e. surrounding more central cells such as Dm4); **arbors overlap considerably**	Dorsal and ventral MCBR; ~ 50 cells per OL	Larger size and additional more distal branches unique among M3B Dm neurons Some cells have occasional processes into the proximal medulla; we included Dm20 in the Dm group since these inner medulla processes appear to be sporadic and were not observed in all Dm20 cells	

1. Fischbach KF & Dittrich APM (1989) The Optic Lobe of Drosophila-Melanogaster .1. A Golgi Analysis of Wild-Type Structure. *Cell Tissue Res* 258(3):441-475.
2. Morante J & Desplan C (2008) The color-vision circuit in the medulla of Drosophila. *Current biology : CB* 18(8):553-565.
3. Takemura SY, *et al.* (2013) A visual motion detection circuit suggested by Drosophila connectomics. *Nature* 500(7461):175-181.
4. Gao SY, *et al.* (2008) The Neural Substrate of Spectral Preference in Drosophila. *Neuron* 60(2):328-342